Title

The high frequency attenuation parameter in NGA-West3 EAS: Modeling κ0 with varying levels of complexity

Authors

Parker, Grace A

Atkinson, Gail M

Baltay, Anne Marie

et al.

Publication Date

2026-07-13

13th National Conference on
EARTHQUAKE ENGINEERING
PORTLAND, OREGON | JULY 13-17, 2026

Resilience Through Community Engagement and Technology

The High Frequency Attenuation Parameter in NGA-West3 EAS: Modeling κ_0 with Varying Levels of Complexity

G.A. Parker[1], G.M. Atkinson[2], A. Baltay[3], D.M. Boore[4], T.E. Buckreis[5] and J.P. Stewart[6]

ABSTRACT

We are developing an earthquake ground-motion model (GMM) for effective amplitude spectra (EAS, the smoothed quadratic mean of two horizontal-component Fourier amplitude spectra) as part of the NGA-West3 project. κ_0 is a model parameter that determines the shape of the high frequency EAS spectrum by controlling how far it deviates from an ω^{-2} source model. We develop κ_0 models within an EAS GMM with increasing levels of complexity: regional constants, regional relationships with the time-averaged shear wave velocity in the upper 30 m (V_{S30}), and modular models based on the depth to the 1 km/s shear wave velocity isosurface (z_1). We estimate regional values of κ_0 between 0.023 and 0.065 s. Mexico, southern California, and Japan have lower than average κ_0 (less attenuation) whereas Taiwan and northern California have higher than average values (more attenuation). We find that sites with low V_{S30} have larger κ_0, whereas κ_0 does not scale with V_{S30} > 300 m/s. Variations in z_1 have a stronger control on κ_0 than V_{S30}, up to a factor of three in some regions; we parameterize a modular z_1 model that can be combined with our $\kappa_0(V_{S30})$ model.

Modeling Workflow

The NGA-West3 project is a large multi-institution effort to develop a global earthquake ground motion database for active crustal regions [1], as well as GMMs for 5%-damped RotD50 pseudo-spectral acceleration and effective amplitude spectra (EAS, the smoothed quadratic mean of two horizontal-component Fourier amplitude spectra). We develop a model for EAS with the primary input parameters of moment magnitude (**M**), Joyner-Boore distance (R_{JB}) and the time-averaged shear-wave velocity in the upper 30 m (V_{S30}), with modeled adjustments to account for regional variations in stress drop, source depth, anelastic attenuation (1/Q), and the high frequency attenuation parameter kappa (κ_0). Our model utilizes seismological theory to constrain terms for geometrical spreading, 1/Q, κ_0, and the spectral shape of the seismic source, and combines them with empirical model terms for the near-source saturation of ground motions, linear site amplification, and basin response [2]. We consider over 91,000 EAS records from 1091 **M** ≥ 3 earthquakes in ten global regions (Fig. 1a). To avoid tradeoffs between components, we use the following multi-phased model fitting approach:

[1] Research Geophysicist, U.S. Geological Survey, Earthquake Science Center, Moffett Field, CA 94035 (email: gparker@usgs.gov)
[2] Professor Emerita, Dept. of Earth Sciences, Western University, London, Ontario, N6A 3K7, Canada
[3] Research Geophysicist, U.S. Geological Survey, Earthquake Science Center, Moffett Field, CA 94035
[4] Scientist Emeritus, U.S. Geological Survey, Earthquake Science Center, Moffett Field, CA 94035
[5] Postdoctoral Scholar, Dept. of Civil and Environmental Engineering, UCLA, CA 90095
[6] Professor, Dept. of Civil and Environmental Engineering, UCLA, CA 90095

Parker GA, Atkinson G, Baltay A, Boore DM, Buckreis TE, Stewart JP. The High Frequency Attenuation Parameter in NGA-West3 EAS: Modeling κ_0 with Varying Levels of Complexity. *Proceedings of the 13th National Conference in Earthquake Engineering*, Earthquake Engineering Research Institute, Portland, OR. 2026.

1. Adjust the EAS amplitude from each record for nonlinear site effects using an existing model [3].
2. Fix the geometrical spreading to decay as $R^{-0.5}$ beyond 50 km based on the decay of surface waves in a half-space [4] using a bilinear function [5]. Use records with $R_{JB} \geq 150$ km to fit regional anelastic attenuation coefficients, parameterized as the inverse of the seismic quality factor (Q), and an initial V_{S30} scaling model using a trilinear form [6], allowing for regional variations in both components. Both 1/Q and V_{S30}-scaling models are fit frequency-by-frequency, and then coefficients are smoothed.
3. Fit near-source saturation [7] and the geometrical spreading using records with $R_{JB} \leq 50$ km. These terms trade off against each other, resulting in non-uniqueness. We find that a constant geometrical spreading of R^{-1} works well to fit the data when combined with a near-source saturation model that depends on frequency (f), magnitude, and earthquake source depth [8].
4. Adjust records from step 1 using the path and site models from steps 2-3, and invert adjusted records over all frequencies to estimate event-specific earthquake source parameters (e.g., earthquake corner frequency, f_c [9]), regional amplitude constants, and site-specific κ_0 values (Eq. 1; Fig. 1b) [10] using a mixed-effects regression [11] where earthquake, region, and station are used as grouping factors.

The parameter κ_0 controls the decay rate of the acceleration spectrum at high frequencies (Eq. 1, Figure 1b) [10]. Here we focus on using site-specific estimates of κ_0 from step 4 above, which falls within the class of broad-band fitting methods described by [12]. We use these estimates to develop models for median κ_0 that depend on region, V_{S30}, and z_1, here using northern California (NorCal) as an example region.

$$EAS \propto -\pi f \kappa_0 \tag{1}$$

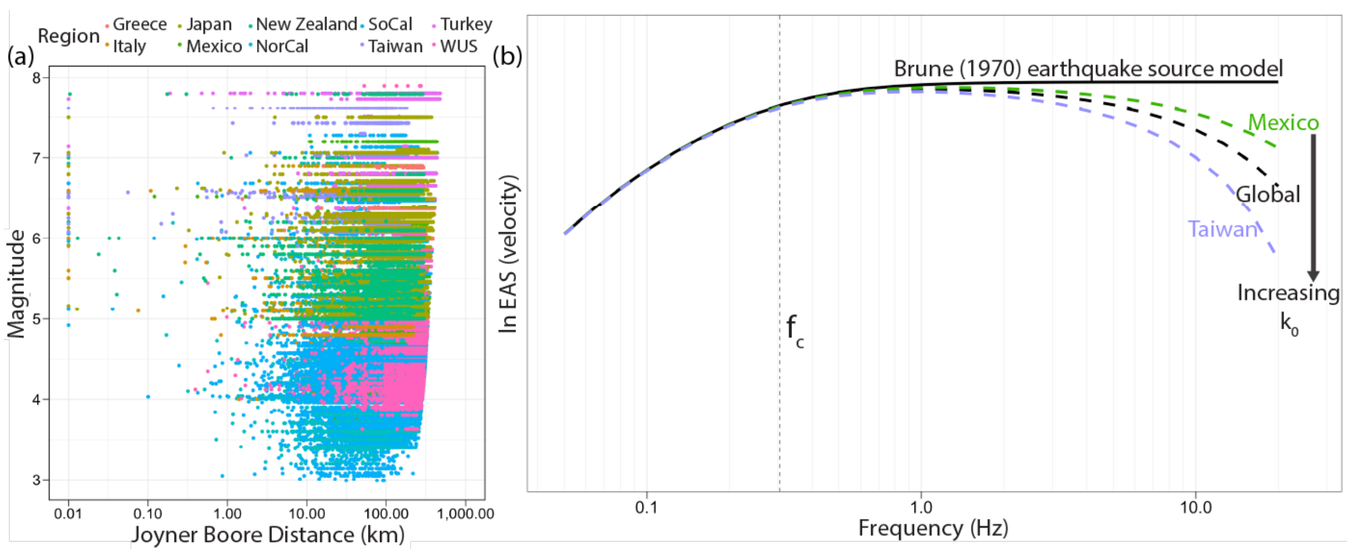

Figure 1. (a) The magnitude-distance distribution of EAS records used in model development, color-coded by earthquake region. SoCal = Southern California; WUS = western United States. (b) Schematic EAS spectra for an **M**6 earthquake showing deviations from an ω^{-2} source model [9] for varying κ_0 values, including the global average and regional endmembers from this study (Fig 2a).

Models for the High Frequency Attenuation Parameter κ_0

We use site-specific estimates of κ_0 to develop several models with varying complexity. The simplest model is a constant value of κ_0 for each region. We find that κ_0 varies from 0.023s in Mexico to 0.065s in Taiwan, with a global average of 0.043s (Fig. 2a). In general, Japan, southern California and Mexico have more high-frequency energy (smaller κ_0 and hence less attenuation), whereas Taiwan and NorCal are more depleted in high-frequency energy with more attenuation (larger κ_0).

V_{S30} - Scaling

We find that there is some correlation between κ_0 and V_{S30} for the softest sites ($V_{S30} \leq 300$ m/s), with softer sites having larger κ_0 (more high frequency attenuation); there is no correlation for sites with $V_{S30} > 300$ m/s (Fig. 2b). We develop region-specific models using a sigmoid function following [5] that increases κ_0 for sites with low V_{S30} (Fig. 2b), fitting coefficients for each region separately. This is consistent with some previous studies that have found no or limited relationships between κ_0 and bedrock velocity for hard-rock sites [12-15] or with V_{S30} [13, 16]. However, there are also studies that have shown a relationship between κ_0 and V_{S30} in the 300-1000 m/s range that we do not see in our data [17, 18, 19]. There are several possible reasons for this difference, including dataset difference (including regional variations) and data sparsity; accuracy of input V_{S30} values; assumptions about site amplification and Q attenuation and their corresponding tradeoffs with κ_0; modeling choices (e.g., we could have fit a linear model across the range of V_{S30}); and differences in κ_0 estimation methods. For example, [17] and [19] use a high-frequency linear fitting approach, whereas this study uses a broadband spectral fitting approach.

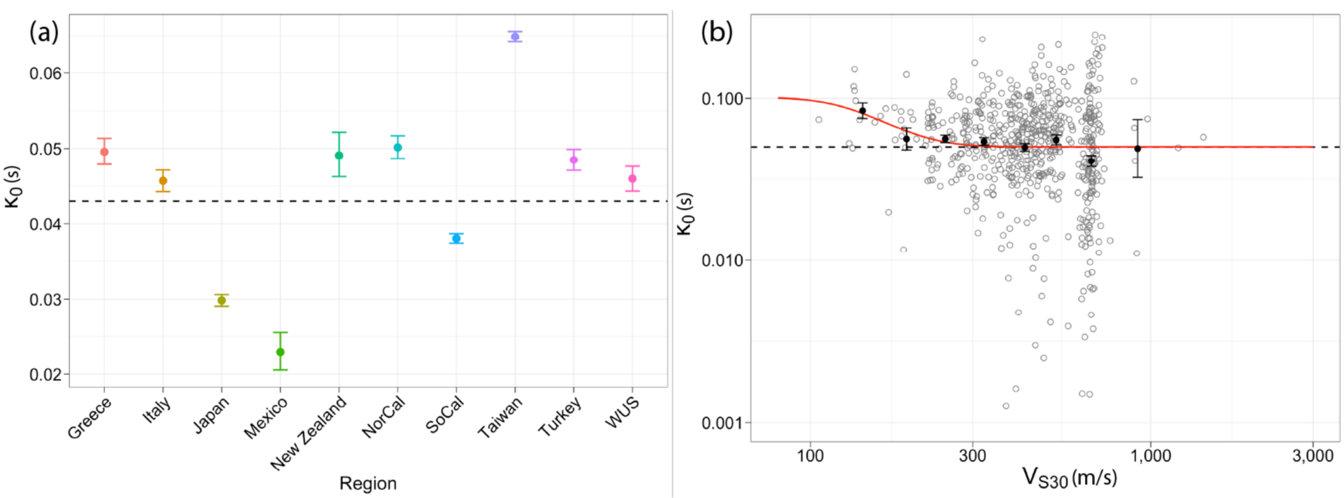

Figure 2. (a) Regional variations in κ_0 shown with ± 1 standard error bars. Black dashed line at the global average value. (b) The relationship between κ_0 and V_{S30} for NorCal. Black points show binned means with ± 1 standard errors, red line shows best-fit sigmoid function, and dashed line shows regional average κ_0 for NorCal (0.05 s).

Relationship With z_1

We find that the depth to the 1 km/s shear wave velocity isosurface (z_1) has a stronger control on κ_0 than V_{S30}. However, we acknowledge that V_{S30} is more readily available from proxy-based models, whereas estimating z_1 requires a site investigation or an available seismic velocity model at the site of interest. Therefore, we parameterize a model for κ_0 using z_1 that can be used in conjunction with the V_{S30}-scaling model if z_1 is known. If z_1 is not known, the $k_0(V_{S30})$ model can be used independently. To do this, we develop a centering model between z_1 and V_{S30} for each region using a sigmoid function following [6] (Fig. 3a). We do not recommend this model to predict z_1, but to account for correlation between the V_{S30} and z_1 model terms.

$$\delta z_1 = \ln(z_1) - \ln(\bar{z_1}) \qquad (2)$$

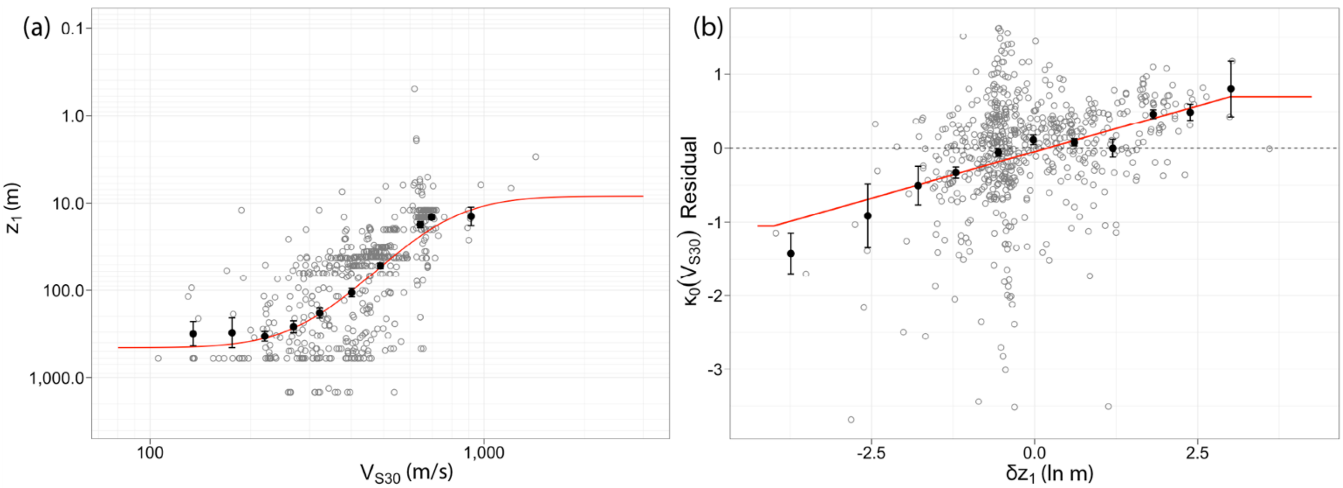

Figure 3. (a) The best-fit sigmoid centering model (red) to account for correlation between V_{S30} and z_1 in NorCal. (b) The trilinear $\kappa_0(\delta z_1)$ model for NorCal based on residuals of the $\kappa_0(V_{S30})$ model, in natural logarithm units. In both panels black points show binned means with ± 1 standard error of the mean. In (b) black dashed line shows 0 for reference.

We subtract the $k_0(V_{S30})$ model from our site-specific k_0 estimates, and fit a model to those values conditioned on δz_1 (the ln difference between the z_1 at a site and the average value $\overline{z_1}$ given the V_{S30} at the site, Eq. 2). We model $\kappa_0(\delta z_1)$ as a trilinear function [20] (Fig. 3b). We find that variations in z_1 can modify k_0 by up to a factor of three in NorCal. This is consistent with past studies that have found κ_0 to be correlated with sediment thickness [18, 21] and depth to the 2.5 km/s shear-wave velocity isosurface [19], but here we offer a more sophisticated parameterization based on δz_1 that takes into account any correlation between z_1 and V_{S30}.

Conclusions

Based on estimates of site-specific κ_0 from the NGA-West3 database, we find that Japan, southern California, and Mexico have smaller than average κ_0 leading to larger high frequency ground motions, whereas Taiwan and NorCal have larger than average κ_0 leading to a relative depletion of high frequency energy. Our results show that κ_0 and V_{S30} are correlated for sites with $V_{S30} \leq 300$ m/s; for sites with larger V_{S30} we find no correlation. This is consistent with some previous studies investigating the relationship between κ_0 and V_{S30} [12-16], however, unlike some past studies [17-19], we do not see a trend with κ_0 across the entire range of V_{S30} considered. This may be due to dataset or methodology differences (e.g., high frequency linear fitting versus broadband spectral fitting [12]). Additionally, in estimating κ_0 we assume a V_{S30} - dependent linear site amplification that may already include implicit κ_0 effects (step 4, above), although we constrain the VS30-scalign to be 0 for frequencies ≥ 12.5 Hz. We also find that sites with deeper than average z_1 have larger κ_0, and sites with shallow z_1 have smaller κ_0, indicating that thicker sediment columns increase high frequency damping. This is consistent with previous findings that investigated the correlation between κ_0 and sediment depth [18, 19, 21], but here we parameterize a model for κ_0 on δz_1 (Eq. 2) such that it can be used in conjunction with our $\kappa_0(V_{S30})$ model, accounting for any correlation between the two site condition parameters. The κ_0 can then be estimated using the sum of either the regional constant or the $\kappa_0(V_{S30})$ with the $\kappa_0(\delta z_1)$ term if z_1 is available. Going forward, we will consider interpolating our site-specific κ_0 to generate spatially continuous maps. Combining all κ_0 models presented here with the linear site response model developed in step 2 above will ensure high frequency spectral shapes consistent with our other GMM components.

References

1. Buckreis TE, Stewart, JP (Eds). Data Resources for NGA-West3 Project. B. John Garrick Institute for the Risk Sciences 2025; Report GIRS-2025-07, doi:10.34948/N3D30R.
2. Parker GA, Atkinson GM, Baltay AS, Boore DM, Buckreis TE, Stewart JP. Preliminary Empirical Models for Effective Amplitude Spectra based on the NGA-West3 Dataset. *SCEC Annual Meeting* 2025; SCEC, Palm Springs, California.
3. Bayless J, Abrahamson NA. Summary of the BA18 ground-motion model for Fourier amplitude spectra for crustal earthquakes in California. *Bull. Seismol. Soc. Am.* 2019; **109** (5): 2088-2105.
4. Ou GB, Herrmann RB. A statistical model for ground motion produced by earthquakes at local and regional distances. *Bull. Seismol. Soc. Am.* 1990; **80** (6A): 1397-1417.
5. Yenier E, Atkinson GM. An equivalent point-source model for stochastic simulation of earthquake ground motions in California. *Bull Seismol. Soc. Am.* 2015; **105** (3): 1435-1455.
6. Parker GA, Stewart JP. Ergodic site response model for subduction zone regions. *Earthq. Spectra* 2022; **38** (2): 841-864.
7. Yenier, E, Atkinson GM. Equivalent Point-Source Modeling of Moderate-to-Large Magnitude Earthquakes and Associated Ground-Motion Saturation Effects. *Bull. Seismol. Soc. Am.* 2014; **104** (3): 1458-1478.
8. Parker GA, Baltay AS, Atkinson GM, Boore DM, Buckreis TE, Stewart JP. A new near-source saturation model for EAS based on the NGA-West3 Database. *SCEC Annual Meeting*, SCEC, Palm Springs, CA, 2024.
9. Brune JN. Tectonic stress and the spectra of seismic shear waves from earthquakes. *J. Geophys. Res.* 1970; **75** (26): 4997-5009.
10. Anderson JG, Hough SE. A model for the shape of the Fourier amplitude spectrum of acceleration at high frequencies. *Bull. Seismol. Soc. Am.* 1984; **74** (5): 1969-1993
11. Bates D, Maechler M, Bolker B, Walker S. Fitting Linear Mixed-Effects Models Using lme4. *J. Stat. Soft.* 2015; **67** (1): 1-48.
12. Edwards B, Ktenidou OJ, Cotton F., Abrahamson NA, Van Houtte C, Fäh D. Epistemic uncertainty and limitations of the κ0 model for near-surface attenuation at hard rock sites. *Geophys. J. Int*. 2015; **202** (3): 1627-1645.
13. Edwards B. Site specific kappa. Technical Report SED/PRP/R/035b/20120410. 2012; Swiss Seismological Service, Zurich, Switzerland.
14. Haendel A, Pilz M, Cotton F. Hard-Rock κ0 at KiK-Net Sites in Japan. *Bull. Seismol. Soc. Am.* 2023; **113** (6): 2650-2665.
15. Palmer SM, Atkinson GM. The high-frequency decay slope of spectra (kappa) for M≥ 3.5 earthquakes on rock sites in Eastern and Western Canada. *Bull. Seismol. Soc. Am.* 2020; **110** (2): 471-488.
16. Nye T, Sahakian VJ, King E, Baltay A, Klimasewski A. Estimates of κ0 and effects on ground motions in the San Francisco Bay area. *Bull. Seismol. Soc. Am.* 2023; **113** (2): 823-842.
17. Van Houtte C, Drouet S, Cotton F. Analysis of the origins of κ (kappa) to compute hard rock to rock adjustment factors for GMPEs. *Bull. Seismol. Soc. Am*. 2011; **101** (6): 2926-2941.
18. Cabas A, Rodriguez-Marek A, Bonilla LF. Estimation of site-specific kappa (κ_0)-consistent damping values at KiK-net sites to assess the discrepancy between laboratory-based damping models and observed attenuation (of seismic waves) in the field. *Bull. Seismol. Soc. Am.* 2017; **107** (5): 2258-2271.
19. Xu B, Rathje EM, Hashash YMA, Stewart JP, Campbell K, Silva WJ. κ0 for soil sites: Observations from Kik-net sites and their use in constraining small-strain damping profiles for site response analysis. *Earthq. Spectra* 2020; **36**(1):111-137.
20. Nweke CC, Stewart JP, Wang P, Brandenberg SJ. Site response of sedimentary basins and other geomorphic provinces in southern California. *Earthq. Spectra* 2022; **38** (4), 2341-2370.
21. Campbell KW. Estimates of shear-wave Q and κ 0 for unconsolidated and semiconsolidated sediments in Eastern North America. *Bull. Seismol. Soc. Am.* 2009; **99** (4): 2365-2392.